ADVANCED HEALTHCARE MATERIALS
www.advhealthmat.de

The Plasticity of Nanofibrous Matrix Regulates Fibroblast Activation in Fibrosis

Yuanbo Jia, Yanzhong Wang, Lele Niu, Hang Zhang, Jin Tian, Dengfeng Gao, Xiaohui Zhang, Tian Jian Lu, Jin Qian, Guoyou Huang,* and Feng Xu**

Natural extracellular matrix (ECM) mostly has a fibrous structure that supports and mechanically interacts with local residing cells to guide their behaviors. The effect of ECM elasticity on cell behaviors has been extensively investigated, while less attention has been paid to the effect of matrix fiber-network plasticity at microscale, although plastic remodeling of fibrous matrix is a common phenomenon in fibrosis. Here, a significant decrease is found in plasticity of native fibrotic tissues, which is associated with an increase in matrix crosslinking. To explore the role of plasticity in fibrosis development, a set of 3D collagen nanofibrous matrix with constant modulus but tunable plasticity is constructed by adjusting the crosslinking degree. Using plasticity-controlled 3D culture models, it is demonstrated that the decrease of matrix plasticity promotes fibroblast activation and spreading. Further, a coarse-grained molecular dynamic model is developed to simulate the cell–matrix interaction at microscale. Combining with molecular experiments, it is revealed that the enhanced fibroblast activation is mediated through cytoskeletal tension and nuclear translocation of Yes-associated protein. Taken together, the results clarify the effects of crosslinking-induced plasticity changes of nanofibrous matrix on the development of fibrotic diseases and highlight plasticity as an important mechanical cue in understanding cell–matrix interactions.

1. Introduction

Natural extracellular matrix (ECM) is usually scaffolded with a crosslinked protein fiber network. Cells attach to the fiber network, perceiving and remolding local microenvironment by interacting with the matrix. When the ECM subjected to strain generated by cells or external forces, fibers will be recruited, aligned, and may undergo permanent displacement or deformation,[1] which is so-called plasticity. Such plastic remodeling of fibrous matrix widely occurs in development, disease, and regeneration, which usually leads to dynamic changes of ECM mechanical properties.[2]

Increasing evidence has shown that the changes of ECM mechanical properties plays a critical role in regulating cell behaviors in various physiological and pathological processes such as fibrosis.[3] As the leading cause of death worldwide, fibrosis is typically characterized by accumulation and overdeposition of fibrous matrix.[3a,4] A variety of studies have demonstrated that the overdeposition of fibrous matrix by fibroblasts leads to an increase of local matrix stiffness (i.e., matrix stiffening), which

Y. Jia, L. Niu, H. Zhang, J. Tian, Prof. X. Zhang, Prof. F. Xu
The Key Laboratory of Biomedical Information Engineering of Ministry of Education
School of Life Science and Technology
Xi'an Jiaotong University
Xi'an 710049, P. R. China
E-mail: fengxu@mail.xjtu.edu.cn

Y. Jia, L. Niu, H. Zhang, J. Tian, Prof. X. Zhang, Prof. F. Xu
Bioinspired Engineering and Biomechanics Center (BEBC)
Xi'an Jiaotong University
Xi'an 710049 P. R. China

Y. Wang, Prof. J. Qian
Department of Engineering Mechanics
Key Laboratory of Soft Machines and Smart Devices of Zhejiang Province
Zhejiang University
Hangzhou 310027 P. R. China
E-mail: jqian@zju.edu.cn

The ORCID identification number(s) for the author(s) of this article can be found under https://doi.org/10.1002/adhm.202001856

Prof. D. Gao
Department of Cardiology
The Second Affiliated Hospital
Xi'an Jiaotong University School of Medical
Xi'an Shaanxi, P. R. China

Prof. T. J. Lu
State Key Laboratory of Mechanics and Control of Mechanical Structures
Nanjing University of Aeronautics and Astronautics
Nanjing 210016, P. R. China

Prof. T. J. Lu
Nanjing Center for Multifunctional Lightweight Materials and Structures
Nanjing University of Aeronautics and Astronautics
Nanjing 21006 P. R. China

Dr. G. Huang
Department of Engineering Mechanics
School of Civil Engineering
Wuhan University
Wuhan 430072 P. R. China
E-mail: gyhuang@whu.edu.cn

DOI: 10.1002/adhm.202001856

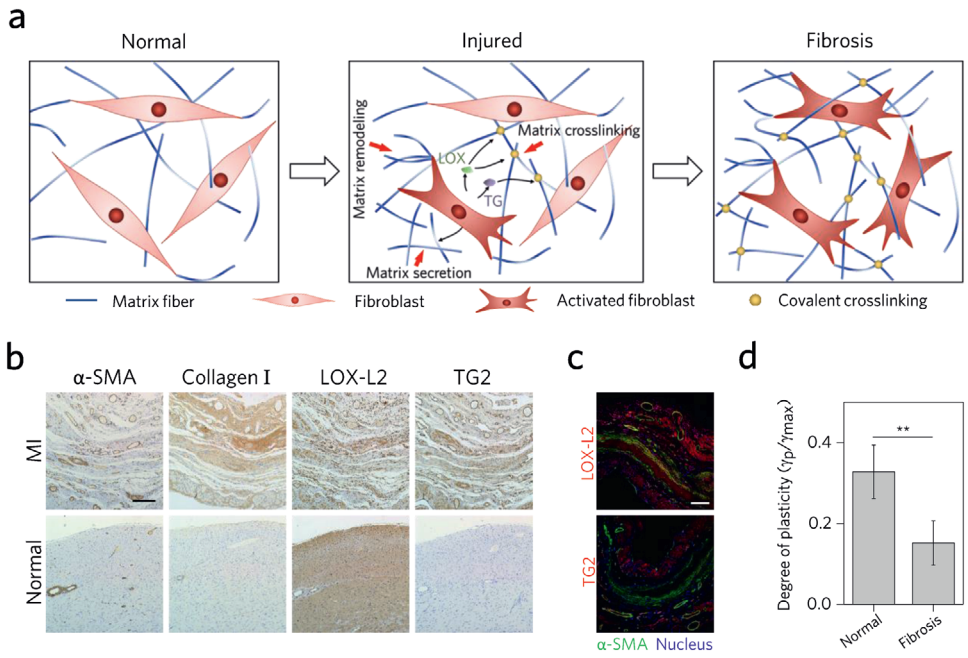

Figure 1. Increased crosslinking degree of extracellular matrix nanofibers in fibrotic tissue leads to mechanical plasticity changes. a) Schematic depicting fibrotic progress in tissues. In injured region, increased secretion of crosslinking enzymes and accumulation of ECM protein will promote fibroblast activation. b) Immunohistochemistry (IHC) analysis of rat myocardial infarction (MI) model show overexpression of collagen I, LOX-L2, TG2 and α-SMA-positive fibroblasts. Tissues were stained with 3,3′-diaminobenzidine (brown) and counterstained with hematoxylin (blue). Scale bar, 200 μm. c) Immunofluorescence staining of LOX-L2, TG2 (red), α-SMA (green), and nucleus (blue) in MI rats. Scale bar, 200 μm. d) Creep and recovery tests characterized mechanical plasticity of normal and fibrotic tissues in heart (rat). Data are shown as mean ± SD; $n = 4$; * and ** indicate $p < 0.05$, $p < 0.01$ by Student's *t*-test.

in turn promotes the proliferation and activation of fibroblasts in a positive feedback manner.[3b,5] Meanwhile, overproduction and activation of crosslinking enzymes, such as lysyl oxidase (LOX) family of enzymes[6] and transglutaminase (TG),[7] have been considered to contribute to matrix stiffening by enhancing mechanical stability of the ECM through increased covalent crosslinking.[7–8] While ECM elasticity has been extensively investigated, much less attention has been paid to the change of ECM plasticity in fibrosis and the effect of it, even though plastic remodeling of fibrous matrix is a common phenomenon in fibrosis.

Recent studies have shown that the native ECM and various cell culture materials are viscoplastic and such mechanical property can play important roles in pathological processes (e.g., cancer invasion[9]). Besides, covalent crosslinking of collagen leads to a decrease of viscoplastic properties.[2,10] Although the effect of matrix plasticity in cell mechanosensing has not been explored, it is recently demonstrated that cells need to generate sufficient traction force to ensure the ability of sensing matrix stiffness, while in viscoelastic materials cells may lose such ability due to mechanical relaxation of the matrix.[11] These lead us to point to a hypothesis that increased covalent crosslinking of fibrous matrix in fibrosis may not only facilitate matrix deposition, but also decrease matrix mechanical plasticity, thus enhancing cell-matrix interaction and thereby promoting fibroblast activation and fibrosis development (**Figure 1**a). Here we investigated the roles and activation mechanisms of mechanical plasticity of fibrous matrix in fibrosis independently from matrix stiffness.

2. Plasticity Changes in Native Fibrotic Tissues

To assess the change of mechanical plasticity in native fibrotic tissues, we first established a rat model with myocardial fibrosis as induced by myocardial infarction (MI). We characterized the expression of crosslinking enzymes (LOX-L2 and TG2) in rat myocardial tissues by immunohistochemistry and immunofluorescence staining, which are considered as attractive therapeutic targets for various fibrotic diseases.[8b,12] We observed that LOX-L2 and TG2 expressions, associated with collagenous matrix and α-smooth muscle actin (α-SMA)-positive fibroblasts respectively, were enriched in infarction regions of MI hearts as compared with normal hearts (Figure 1b,c). Immunohistochemical staining showed that LOX-L2 was expressed in normal myocardial tissue, similar to previous work in literature.[6] Fluorescence staining of the entire heart section also showed high expressions of α-SMA, LOX-L2 and TG2 in infarction regions in contrast with non-infarction regions (Figure S2, Supporting Information). These results indicate an increased matrix crosslinking in fibrosis regions.

We then characterized the plastic property of normal and fibrotic tissues using creep and recovery tests. For this, constant stress was applied to tissue samples for 100 s and the strain could recover for 1000 s. Results showed that fibrotic myocardial tissues exhibited significantly decreased mechanical plasticity in term of unrecoverable deformation compared to normal myocardial tissues (Figure 1d). Since covalent crosslinking of collagen has been found to result in decreases material viscoplastic

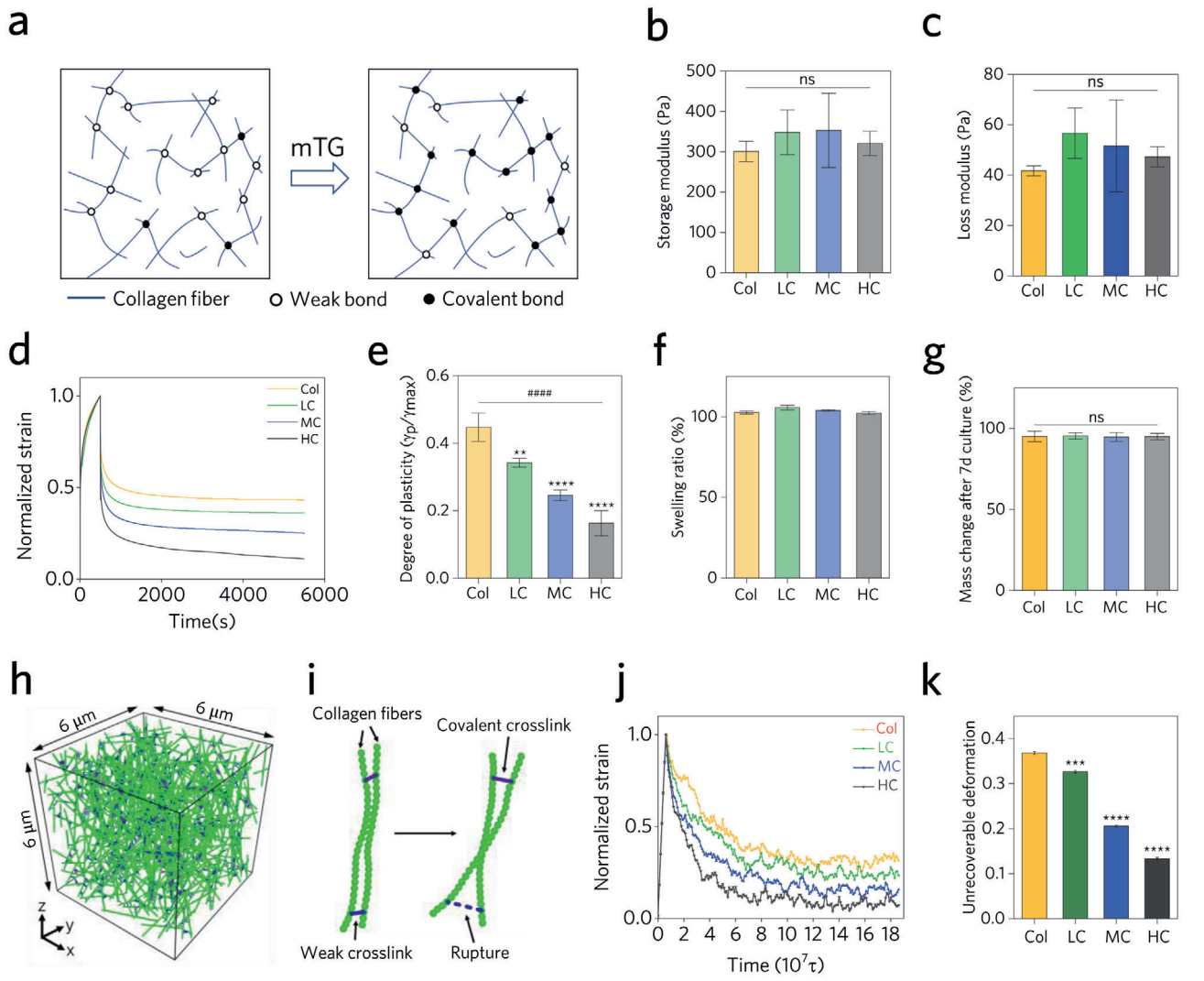

Figure 2. Mechanical plasticity of nanofibrous collagen is independently tuned by covalently crosslinking using mTG. a) Schematic depicting the collagen covalently crosslinked by mTG. Hollow circle indicates weak bond in self-assembled collagen, while solid circle indicates strong covalent bond. b,c) Storage and loss moduli do not show significant difference. ns, not significant by one-way ANOVA. d)) Creep and recovery tests showed that plasticity of collagens can be regulated by different treatment time of mTG. e) Plasticity of collagen quantified from creep and recovery tests. ** and **** indicate significant difference compared to Col with $p < 0.01$ and $p < 0.0001$ by one-way ANOVA, respectively. Mechanical plasticity decreases significantly with the increase of crosslinking time ($^{\#\#\#\#}p < 0.0001$, Spearman's rank correlation). f,g) Swelling and degradation tests of collagens under cell culture condition. h) Schematic of CGMD model for collagen fiber network. i) Collagen fibers are connected by weak (from collagen self-assembly) and strong crosslinks (from mTG treatment). Rupture will happen once the length of weak crosslinks are stretched to a threshold value. j) Simulation of stretch and recovery tests (where τ is time step, Supporting Information). k) Degree of plasticity of collagen quantified from simulation results, in consistency with the experiment data in (e) (results were averaged on three samples over the last $10^6\tau$ in each condition.). For (b), (c), (e), and (f), $n = 5$, data are shown as mean ± SD.

properties,[2,10] our data indicate a probable association between matrix crosslinking and mechanical plasticity in fibrotic tissues.

3. Modulation of Matrix Mechanical Plasticity

To develop a set of nanofibrous matrix with tunable mechanical plasticity, we modulated the covalent crosslinking degree of type I collagen using microbial transglutaminase (mTG). Collagen I is the most abundant matrix protein in mammals as well as the main deposited matrix in fibrotic tissues.[13] Collagen solution can spontaneously form physically crosslinked fibrous hydrogels via self-assembly at physiological temperature and pH, while TGs can covalently crosslink collagen fiber networks by catalyzing the formation of intermolecular ϵ-(γ-glutamyl)lysine bonds.[14] We first prepared a self-assembled collagen hydrogel (pure collagen, Col) at a final concentration of 5 mg mL^{-1} and then soaked the hydrogel in 0.1% mTG solution for 1 h (low covalently crosslinked collagen, LC), 3 h (medium covalently crosslinked collagen, MC) or 5 h (high covalently crosslinked collagen, HC), respectively, to covalently crosslink it (**Figure 2**a). Since the fiber structure of the collagen hydrogels was formed in the self-assembly step, treating with mTG did not change hydrogel microstructural features.

This was confirmed by rheological measurement, where the storage modulus of the different covalently crosslinked hydrogels was maintained around 320 Pa (Figure 2b, and Figure S3a, Supporting Information), similar to native normal tissues but much lower than that of native fibrotic tissues (about 10–20 kPa).[15] At such stiffness level, the cultured fibroblasts will not be activated so that the effects of matrix stiffness can be eliminated. Shear loss modulus also did not show significant difference for different covalently crosslinked collagen hydrogels (Figure 2b).

To characterize the mechanical plasticity of the hydrogels, creep and recovery tests were applied. A constant stress of 20 Pa was applied to the hydrogel samples for 500 s, considering that cells usually exert traction forces on the ECM on a timescale of seconds to minutes.[16] After the stress was relaxed for 5000 s, collagen hydrogels exhibited decreased unrecoverable deformation (i.e., decreased mechanical plasticity) with the increase of covalent crosslinking degree (Figure 2d,e). Using annular-shaped hydrogels, tensile experiments were carried out to verify the permanent deformation of the hydrogels under long-term recovery. The results showed that the trend of decreased permanent deformation existed even after 7 d's recovery (Figure S4, Supporting Information). MC and HC hydrogels showed a significant lower irreversible deformation after 7 d compared to 10 min's recovery, while deformation of Col and LC hydrogels did not change much. The results of swelling and degradation experiments did not show significant differences among the hydrogels under cell culture condition (Figure 2f,g). In combination, these results demonstrate that our approach can construct collagen hydrogels with tunable plasticity, but similar initial modulus, swelling ratio and degradability.

To uncover the underlying mechanism that connects the macroscopic plasticity of collagen hydrogel and microscopic crosslinking degree, we established a coarse-grained molecular dynamics (CGMD) model to simulate fiber network behaviors under deformation and relaxation. Collagen hydrogel was modeled as a 3D random network of crosslinked fibers (Figure 2i), where the involved parameters (e.g., fiber diameter, length, stiffness and density) were given according to published experiments.[17] Prior studies suggested the irreversible sliding fibers or the formation of new crosslinks contribute to the plasticity of collagen networks.[18] Considering the irreversible sliding of fibers and simplification of simulations, we postulated that the weak crosslinks (mainly hydrogen bond interaction) in self-assembled collagen can be easily broken under stress, leading to irreversible slippage between matrix fibers, while the presence of strong covalent crosslinks can keep the integrity of collagen network, resist such slippage, and help the fibrous network to restore its original state after stress is removed. In the CGMD model, the mechanical properties of the weak crosslinks and strong crosslinks were distinguished by adopting different parameters in a harmonic description. When the deformation at crosslinking sites exceeds a certain threshold, the weak crosslinks will rupture while the strong crosslinks will not (Figure 2i). The density of weak crosslinks (from self-assembly of collagen) is fixed, while the density of strong crosslinks is proportional to the treatment time of mTG. More detailed description of the model can be found in Supporting Information. We duplicated the relaxation tests by applying displacement load to the 3D network until the tensile strain reached about 30% and then relaxed it. The time-dependent strain of the network was obtained through the simulations (Figure 2j,k). In agreement with our experiments, the simulation results also showed decreased unrecoverable deformation in collagen hydrogels with the increase of strong crosslink density.

4. Matrix Plasticity Regulates Activation and Morphology of Fibroblasts

Next, we investigated the effect of matrix plasticity on phenotypic transformation of fibroblasts. We first respectively encapsulated primary cardiac fibroblasts (CFs) and lung fibroblasts (LFs) in 5 mg mL^{-1} self-assembled collagen, and then treated the hydrogels with 0.1% mTG for different durations. Phenotypic transformation of fibroblasts was assessed with immunofluorescence staining for α-SMA after 7 d of culture. In Col hydrogels, fibroblasts showed little expression of α-SMA (**Figure 3**a), which matches the previously reported experiments.[19] Strikingly, as the mechanical plasticity of collagen was decreased by increasing covalent crosslinking, obvious expression of α-SMA was observed (Figure 3a). To further verify these results, we measured the mRNA expression of α-SMA and found significant correlation between matrix plasticity and α-SMA expression ($p < 0.0001$, Spearman's rank correlation, Figure 3b). We further constructed another two sets of hydrogels using 1 and 3 mg mL^{-1} collagen hydrogels with stroage modulus of about 32 and 156 Pa, respectively (Figure 3b,c, Supporting Information). We observed that CFs in these two sets of hydrogels both showed increased α-SMA expression with the decrease of matrix plasticity as reflected by the results from immunofluorescence staining and RT-PCR (Figure S5a–c, Supporting Information).

To assess the effect of mTG on fibroblasts, cells were pretreated with 0.1% mTG for 5 h before encapsulation, and no significant difference was observed compared to the Col group (Figure S6a, Supporting Information). Previous work has shown that matrix degradation has an important role in mechanosensing of cells.[20] To assess the effect of matrix degradation in this work, we used GM6001 to widely inhibit matrix metalloproteases and observed similar results (Figure S6b,c, Supporting Information). To verify the universality of the 3D results, we also cultured cells on the surface of constructed matrix and observed similar phenomenon (Figure S7a, Supporting Information). Since hydrogels were constructed before cells were seeded in 2D culture, the effect of mTG on fibroblasts can be further eliminated on the other hand. Thus, the effect of matrix plasticity on fibroblast activation is similar in both 2D and 3D cultures and is independent of mTG and matrix degradation. These results highlight the influence of mechanical plasticity on fibrosis development independent of stiffness.

Interestingly, different cell morphologies were also observed in hydrogels with different plasticity or collagen concentration. Fibroblasts (both CFs and LFs) exhibited larger spreading areas in hydrogels with lower mechanical plasticity or lower collagen concentration (Figure 3d,e, Figure S5d,e, Supporting Information), same as cells cultured on 2D hydrogels (Figure S7b,c, Supporting Information). A possible explanation is that in high plastic collagen weak crosslinked bonds can be easily broken, leading to slippage between the fibers and failing to provide robust resistance to cell traction. Thus, at the same collagen concentration, cells can generate greater traction force in hydrogels with lower

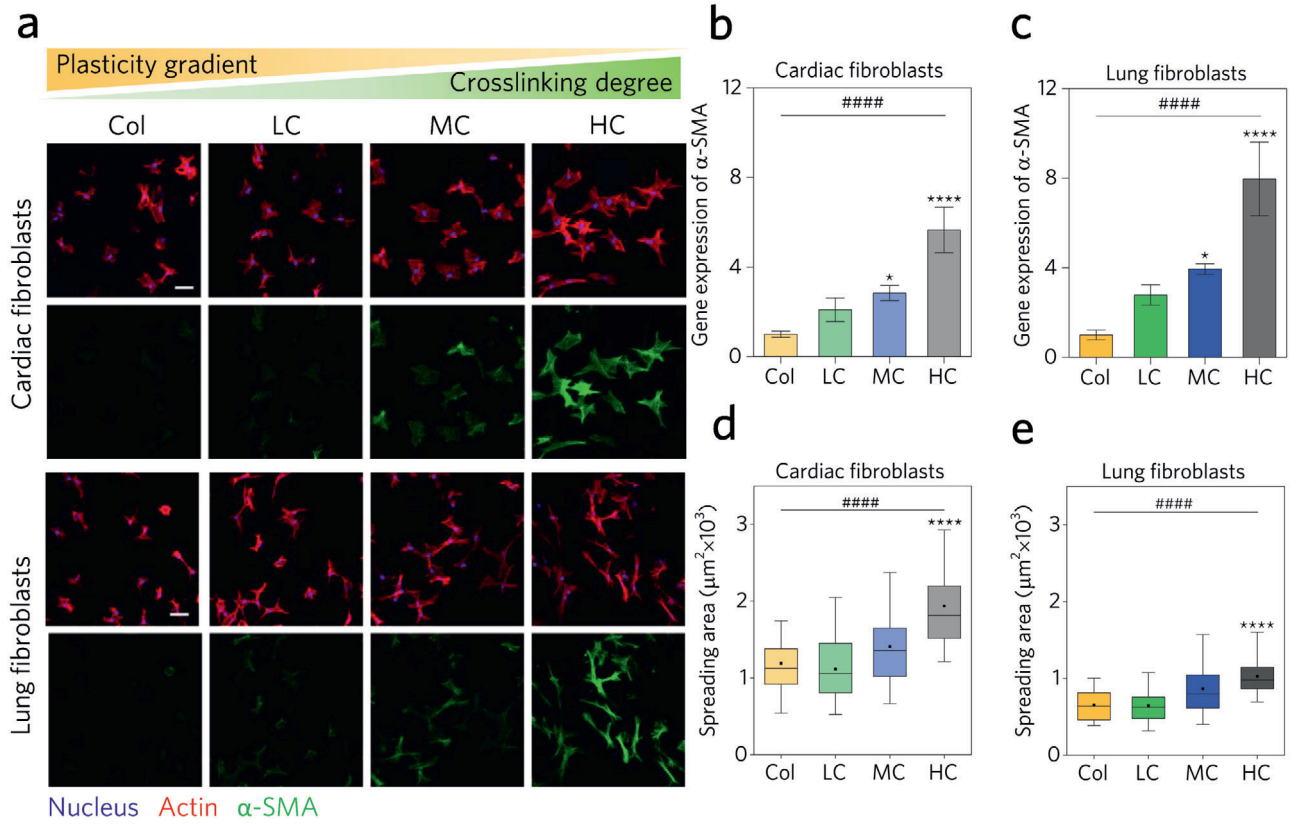

Figure 3. Decrease of mechanical plasticity promotes activation and spreading of fibroblasts in 3D hydrogels. a) Immunofluorescence of cardiac fibroblasts and lung fibroblasts encapsulated within 5 mg mL^{-1} collagen gels with different mechanical plasticity, showing the expression of α-SMA increases with the decrease of collagen plasticity (blue, nucleus; red, actin; green, α-SMA). Images were taken after 7 d of culture. Scale bars, 50 μm. b,c) Quantitative real-time PCR analysis of gene expression of α-SMA in CFs and LFs after 7 d of culture. Values are normalized by gene expression levels measured in Col hydrogels. $n = 3$. Data are shown as mean ± SD. d,e) Quantification of cell spreading area from immunofluorescence images. The box plots show 25/50/75th percentiles and whiskers show 5/95th percentiles. Black dots represent the mean of the data, $n > 50$ cells. From (b) to (e), * and **** indicate $p < 0.05$ and $p < 0.0001$ by one-way ANOVA, respectively. #### indicates $p < 0.0001$ by Spearman's rank correlation.

plasticity and thereby tend to spread with a larger area. The difference of cell spreading area in different concentrations of collagen may be due to steric hindrance.[21]

5. Cytoskeletal Tension Mediates the Mechanotransduction of Matrix Plasticity in Fibroblasts

Since it has been reported that the activation of fibroblasts can be mediated by cytoskeletal tension,[22] the above results lead us to the hypothesis that matrix plasticity may affect the morphology and activation of fibroblasts by regulating cytoskeletal tension. To test this hypothesis, we first examined the formation of focal adhesion complexes using antibody of paxillin and vinculin. It has been reported that within an appropriate stiffness range, focal adhesions are more likely to mature on stiffer substrates because of a higher stress level of actin filaments.[23] Indeed, CFs encapsulated in collagen hydrogels showed increased adhesion numbers and length with the decrease of matrix plasticity (**Figure 4**a–c). Similar results were also observed in CFs cultured on 2D hydrogels (Figure S8, Supporting Information).

We next investigated the pathways by which cells sense mechanical plasticity of the matrix. It is generally believed that cells perceive mechanical stimulation from their microenvironment through adhesions and plasma membranes and transmit mechanical signals to the nucleus through actin fibers and other enzymatic reactions. To verify related pathways, we blocked the mechanotransduction pathways of CFs in HC hydrogels using antibody for β1 integrin,[24] losartan potassium for angiotensin II type I receptor (AT_1R, a force-sensing receptor on cell membranes[25]), blebbistatin for myosin II ATPase to inhibit myosin-based contractility, and Latrunculin A (LAT-A) for G-actin to inhibit actin polymerization, respectively. All these treatments decreased the expression of α-SMA compared with the HC group (Figure 4d,e). Interestingly, inhibition of AT_1R seemed to be not as effective as other approaches, indicating that integrin-actin pathway could be the main mechanotransduction pathways in our experiments. Further, we used Rho activator II to increase cytoskeletal tension of CFs in Col and HC hydrogels. Strikingly, we observed that α-SMA expression of treated CFs in Col hydrogels slightly increased compared to untreated groups, while showed a significant increase in HC hydrogels (Figure S9, Supporting Information). This indicates a potential mechanism that high plastic hydrogels could not provide sufficient resistance against cell traction so that a robust interaction between cells and matrix cannot be formed despite that cell contractility has been activated by

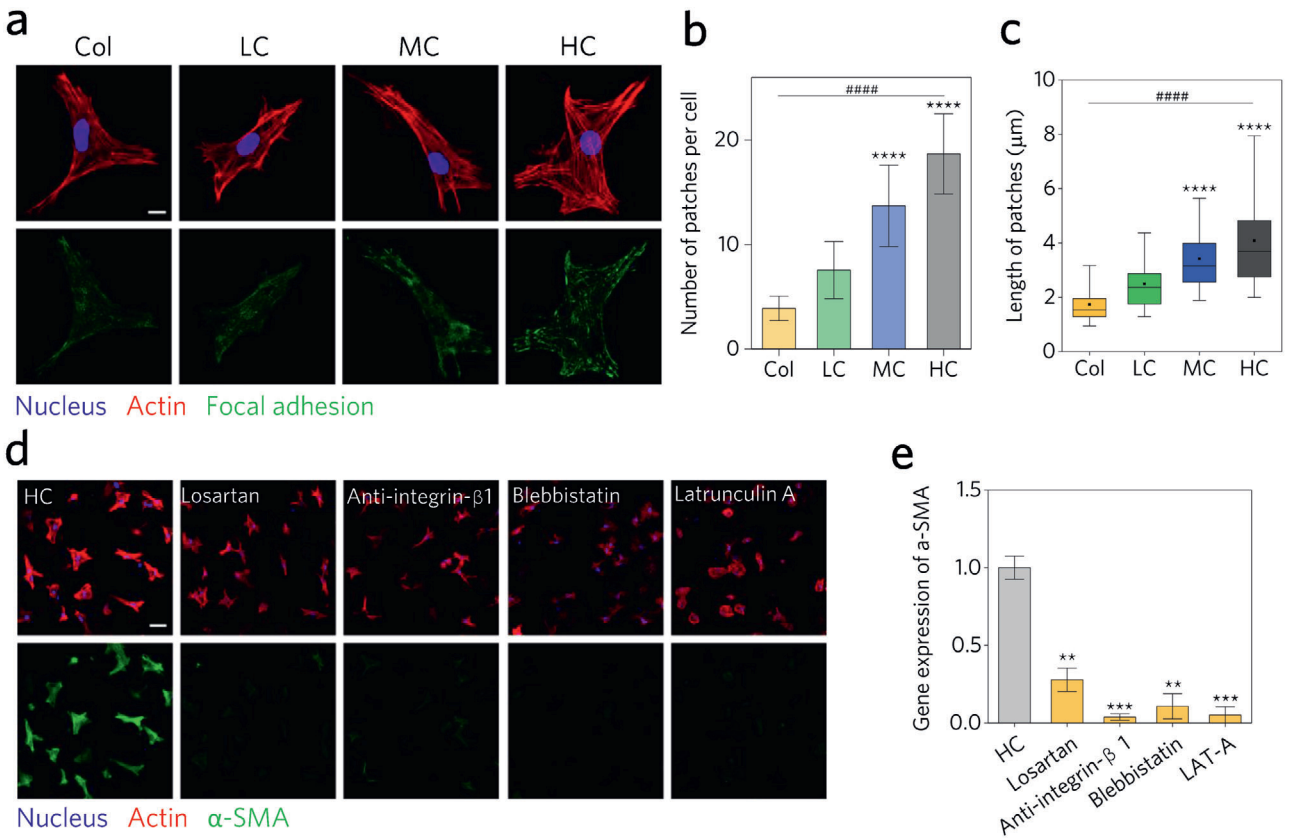

Figure 4. Matrix plasticity regulates fibrosis by cell contraction in 3D hydrogels. a) Immunofluorescence stain for focal adhesion (paxillin and vinculin, green), nucleus (blue), and actin (red) in CFs cultured in 5 mg mL^{-1} 3D collagen hydrogels for 7 d. Scale bar, 20 μm. b) Quantification of the number of mature focal adhesions per cell. Data are shown as mean ± SD. $n = 8$ cells. c) Quantification of the length of focal adhesions. The box plots show 25/50/75th percentiles and whiskers show 5/95th percentiles. Black dots represent the mean of the data. $n \geq 35$ adhesions from the 8 cells quantified in (b). For (b) and (c), **** indicates $p < 0.0001$ by one-way ANOVA. #### indicates $p < 0.0001$ by Spearman's rank correlation. d) Immunofluorescence of CFs in HC hydrogels treated with losartan potassium, integrin $\beta 1$ antibody, blebbistatin, and latrunculin A (blue, nucleus; red, actin; green, α-SMA). Scale bar, 50 μm. e) Gene expression of α-SMA in CFs cultured in HC hydrogels with various treatments. Values are normalized by gene expression levels measured for HC hydrogels. ** and *** indicate $p < 0.01$ and $p < 0.001$, respectively (Student's t-test). $n = 3$. Data are shown as mean ± SD.

treatment.[26] All these results indicate that cytoskeletal tension and cell-matrix interaction play a critical role in matrix plasticity-mediated fibroblast activation.

6. Modeling and Simulations Verify the Important Effect of Matrix Plasticity on Cell Traction

To further prove our hypothesis, we developed a quasi-2D model to simulate the contraction process of a cell cultured in nanofibrous collagen matrix (**Figure 5**a). The ECM was modeled as a quasi-2D random network of crosslinked collagen fibers, in which the parameters of fibers and crosslinking are the same as those in the 3D CGMD model. The cell located at the circular region in the center applied contractility to the matrix by imposing displacement in radial direction (red annulus in Figure 5a). The resultant contraction force was quantified by integration of the radial force of the annular region during the contraction process, and the contraction strain was measured by the shrinkage of the circle diameter. Under quasi-static loading, the observed force-strain relationships suggested that cell traction force was significantly enhanced with the decrease of matrix plasticity (Figure 5b). Our simulation results match the previously reported range of traction forces of single cells in collagen (several nanonewtons).[27]

We also applied a non-quasi-static fast loading for the same region and direction (red annulus in Figure 5a) and then held at the strain plateau to simulate the scenario of relaxation. Cell traction experienced two stages of ascending and relaxing, and showed distinct stress levels in Col and HC hydrogels all the time (Figure 5c). Furthermore, we calculated the stretching energy (the total harmonic stretching potential energy, Supporting Information) of individual fibers in Col and HC hydrogels during the cell contraction process (Figure 5d) and analyzed the spatial distribution of stretching energy in the collagen networks. Under 30% strain, stretching energy distribution of the fibers in Col hydrogels remained at a relatively low level (Figure 5e), while the fraction of fibers with energy higher than 80 $k_B T$ significantly increased in HC hydrogels (Figure 5f). Similar results can be found in bending energy distribution (Figure S10, Supporting Information). Meanwhile, statistics of the permanent displacement of collagen fibers around the cell after a long relaxation showed a larger plastic deformation in Col network than

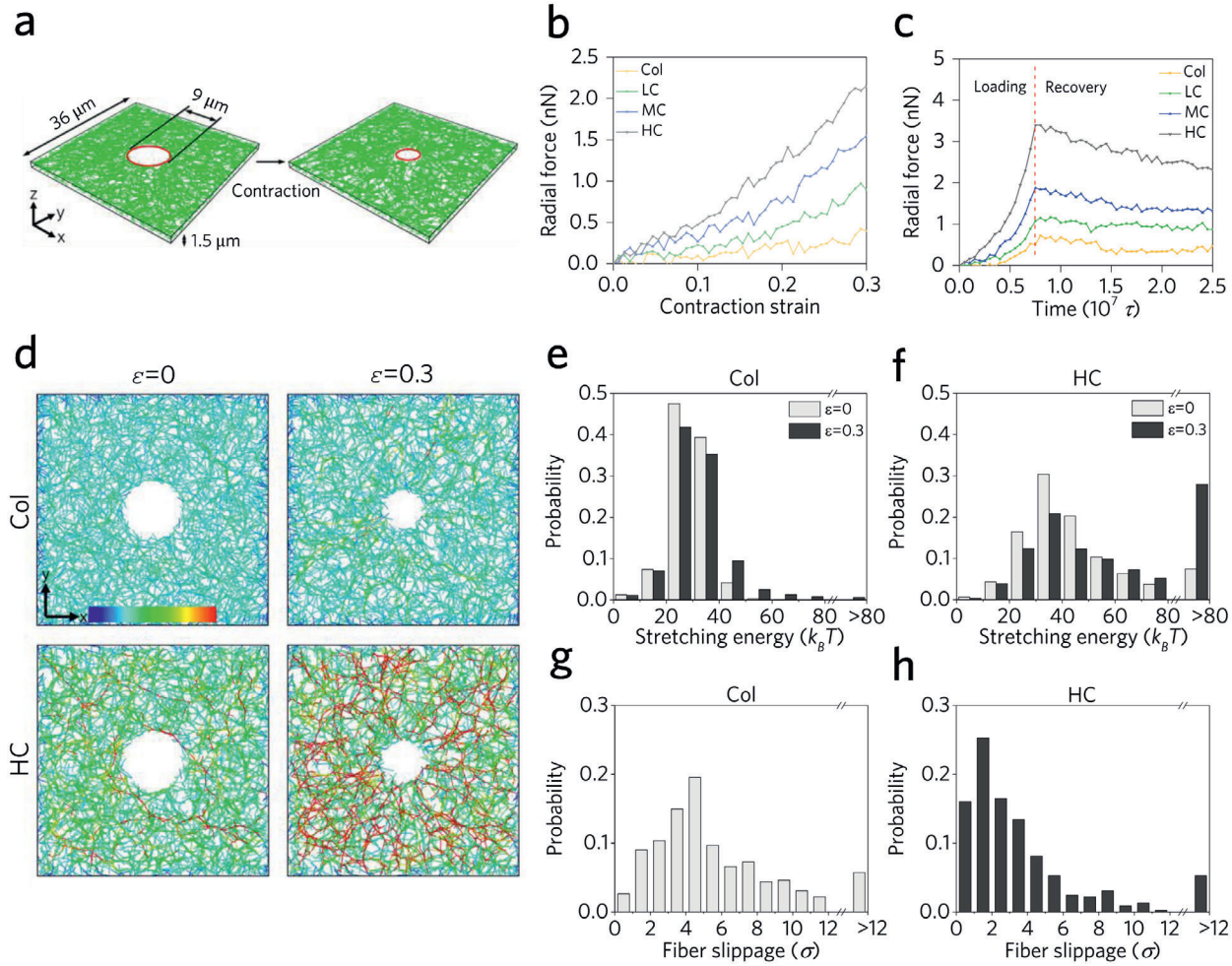

Figure 5. 2D CGMD model for cell contraction in fibrous ECM. a) Schematic of cell contraction process in 2D CGMD model. The circular region represents the cell and contractility is applied to the collagen matrix by a displacement loading in radial direction. b) Quasi-static loading results for force and strain relation during cell contraction process. c) Non-quasi-static fast loading to assess stress relaxation of matrix after cell contraction. d) Snapshots of Col hydrogels (left) and HC hydrogels (right) at initial (top) and final (bottom) states during cell contraction process. Colors are assigned according to the stretching energy in the collagen fibers. Color bar, 0–100k_BT. e,f) Stretching energy distribution of collagen fibers in Col and HC hydrogels during cell contraction process. Class interval is 10k_BT. Data > 80k_BT are counted together in order to facilitate the display. g,h) Quantification of fiber permanent slippage after cell contraction is removed. $\sigma = 60$ nm. Fiber slippage is calculated as the distance between the midpoints of each fiber before and after deformation. Only fibers within two times of cell radius from the center were calculated. Data >12σ are counted together in order to facilitate the display.

that in HC network (Figure 5g,h). These results indicate that for collagen hydrogels without covalent crosslinking, the energy of cell contraction is largely dissipated by breaking of the weak crosslinks, resulting in long-term plastic deformation and low cell traction force within the fibrous networks; however, for covalently crosslinked collagen hydrogels (by mTG treatment), the introduction of strong crosslinks allows cell contraction energy to be easily stored in the intact fiber networks and thus the cell can produce an elevated traction force.

7. YAP Works as a Key Downstream Molecule in Fibroblast Activation

After elucidating the physical mechanism of matrix plasticity affecting fibroblast fate and function via cytoskeletal tension, we further investigated the downstream molecular mechanism. Yes-associated protein (YAP), as a transcription coactivator, has been recently found to read diverse mechanical and cytoskeletal cues to regulate gene expression for driving various cell behaviors.[28] Recent studies have also found that the expression and nuclear translocation of YAP have a positive effect on fibrosis as induced by the increased matrix stiffness.[29] Consistent with the result of enhanced α-SMA expression, nuclear translocation of YAP increased in CFs with decreasing matrix plasticity after 7 d's culture (**Figure 6**a,b). The ratio of YAP in nucleus to cytoplasm in 2D cultured cells showed similar trend and seemed to be larger than that in 3D cultured cells at the same level of plasticity (Figure S11, Supporting Information). One possible speculation is that cells cultured in 2D are more likely to form highly tensed actin-cap, which plays a positive role in YAP nuclear translocation.[30] To test

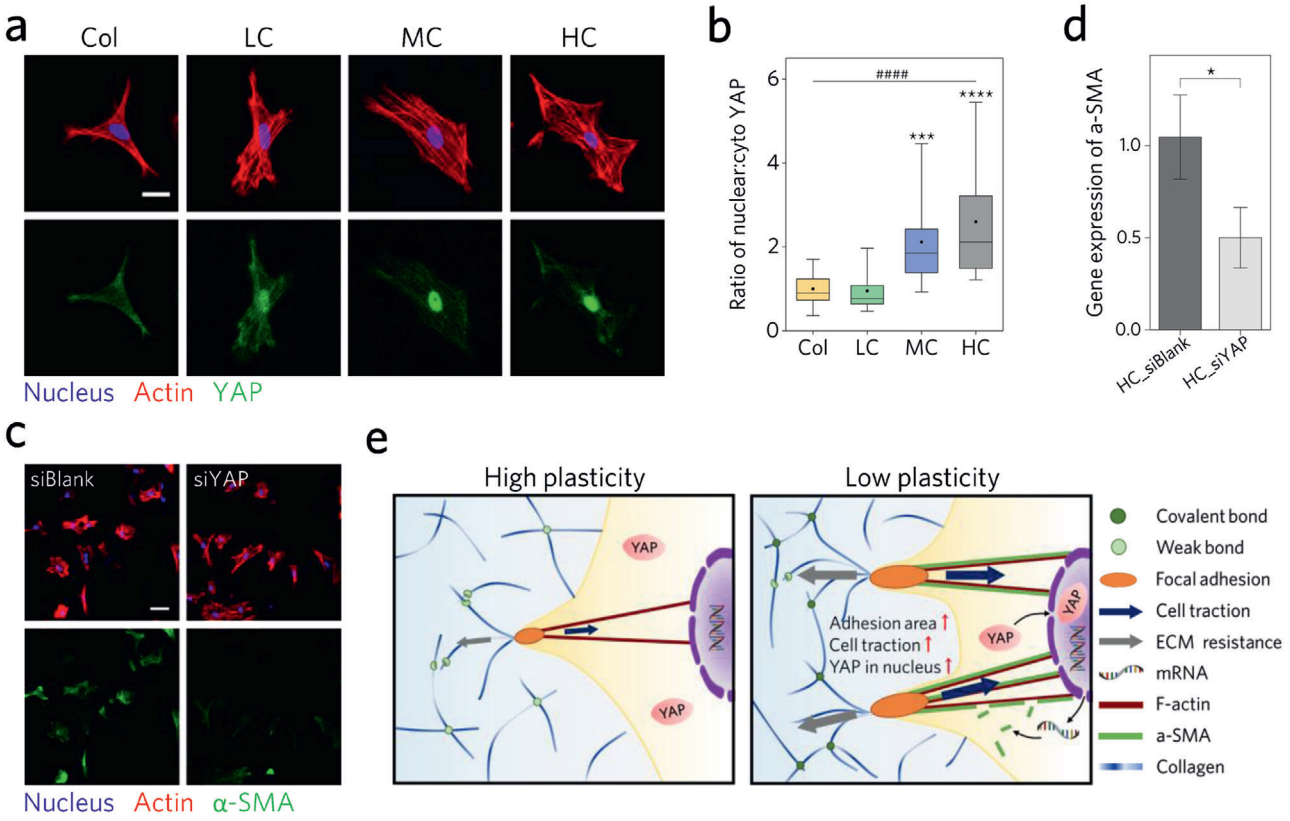

Figure 6. Nuclear translocation of YAP in CFs increases with the decrease of matrix plasticity. a) Immunofluorescence stain for YAP (green), nucleus (blue), and actin (red) in CFs cultured in 5 mg mL^{-1} collagen hydrogels for 7 d. Scale bar, 20 μm. b) Quantification of the ratio of nuclear YAP to cytoplasmic YAP for cells. Values are normalized to cells cultured in Col hydrogels. $n > 40$ cells. *** and **** indicate $p < 0.001$ and $p < 0.0001$ by one-way ANOVA. #### indicates $p < 0.0001$ by Spearman's rank correlation. The box plots show 25/50/75th percentiles and whiskers show 5/95th percentiles. Black dots represent the mean of the data. c) Immunofluorescence of CFs cultured in HC hydrogels with small interfering RNA (blue, nucleus; red, actin; green, α-SMA). Scale bar, 50 μm. d) Gene expression of α-SMA. Values are normalized by gene expression levels measured in meaningless RNA sequence treatment group. * indicates $p < 0.05$ (Student's t-test). $n = 4$. Data are shown as mean ± SD. *** and **** indicate $p < 0.001$ and $p < 0.0001$, respectively (Student's t-test). e) Schematic depicting how matrix plasticity regulates fibroblasts activation. Fibroblasts extend pseudopods in the matrix and perceive the mechanical signal in the environment by adhering to matrix fibers. In high plastic matrix, cell contraction can easily rupture the weak crosslinks, leading to slippage of fibers and insufficient resistance. While in low plastic matrix, matrix fiber network provides sufficient resistance due to the strong covalent crosslinks, thus promotes the formation and maturation of focal adhesions, generation of cytoskeleton tension and nuclear translocation of YAP, all of which finally mediate fibrotic phenotype of fibroblasts.

the role of YAP in matrix plasticity-regulated fibroblast activation, we inhibited YAP expression of CFs cultured in HC hydrogels by small interfering RNA (siRNA) and observed reduced expression of α-SMA (Figure 6c,d). These results indicate that YAP works as a key downstream molecule in CFs activation. Many studies have proven that YAP plays a critical role in mechanotransduction in 2D cultured cells,[31] as well as in 3D cultured cells.[11c] For most 2D systems, YAP nuclear translocation is modulated by actin–myosin contraction and usually increases with increasing matrix stiffness and cytoskeletal tension. However, in 3D cultured systems, there are numerous factors that can influence mechanotransduction pathways, such as confinement, porosity, degradation, stiffness, and viscoelasticity.[32] YAP nuclear translocation is not strictly positively correlated with matrix stiffness and can be modulated by other factors.[33] Besides, breast cancer progression in 3D could be derived through a YAP-independent mechanotransduction pathway.[34] In this work, we demonstrated the role of cytoskeletal tension and YAP in plasticity regulated fibroblast activation. The deeper correlation between these two influencing factors in 3D cultured systems will be an interesting question for further research.

8. Discussion

This work identified the important role of mechanical plasticity of nanofibrous matrix in mediating fibroblast activation. Many existing studies have highlighted the important effects of biochemical cues (e.g., transforming growth factor-β1)[35] and mechanical stiffness on fibroblast activation.[36] Our results indicated that self-assembled fibrous collagen hydrogels showed high plasticity and in which fibroblasts remain undifferentiated. However, when we decreased the plasticity of collagen hydrogels by increasing covalent crosslinking, fibroblasts showed a significant fibrotic response as reflected by the increased α-SMA expression (Figure 3). Since the material systems we constructed have low and the same initial modulus, this process is stiffness independent.

Although it has been reported that covalently crosslinked hydrogels are more difficult to degrade and matrix degradability has an important impact on cell behaviors,[20b] no significant changes of fibroblast activation were observed when matrix metalloproteases were broadly inhibited in our experiments (Figure S6b,c, Supporting Information). Importantly, the hydrogels we constructed showed similar plastic behaviors under creep and recovery tests compared to native normal and fibrotic tissues (Figures 1e and 2e). These highlight the importance of matrix plasticity in mimicking the mechanical microenvironment of native fibrotic tissues.

Mechanistically, we found that the enhanced fibroblast activation in low plastic matrix is mediated through integrin-actin pathway and nuclear localization of YAP (Figure 6e). In high plastic collagen, matrix cannot provide effective resistance to actin contraction because of the rupture of weak crosslinks and the slippage of local fibers. On the contrary, in low plastic collagen, deformation energy can be stored in the network due to the existence of strong covalent crosslinks, thus enabling the build-up of cell traction and the formation of a robust cell-matrix interaction.[2] Experiments of inhibiting or promoting cytoskeletal contractility and CGMD simulation both verified the above points (Figure 5b,c).

2D cultured cells extended a larger spreading area on hydrogels with low plasticity, agreeing with previously reported works,[11a,b] in which cell spreading area on elastic hydrogels is larger than that on stress-relaxed hydrogels with a low ligand density. However, the spreading of 3D cultured cells in our material system showed a trend different from previously reported results of cells cultured in viscoelastic (e.g., alginate,[11c,d,37] poly(ethylene glycol) (PEG)[38] and hyaluronic acid (HA)[39]) or viscoplastic hydrogels (e.g., alginate[9,37]). Cells encapsulated in above-mentioned hydrogels have been found to spread greater when the constructed hydrogels had a faster stress relaxation or lower mechanical plasticity. A recent work constructed a non-degradable alginate that specifically decouples irreversible creep from stress relaxation and modulus.[37] Cell aspect ratio and YAP nuclear translocation reached maximum in the middle plastic group and can be modulated by actin–myosin contraction using various concentrations of blebbistatin. Kinetic Monte Carlo simulations also verified the cell spreading as a function of the matrix plasticity. These results emphasize the importance of cell contraction in matrix plasticity regulated cell behavior. However, in consideration of nonfibrous structure of all the above hydrogels, one possible explanation is that steric hindrance in nonfibrous hydrogels has a greater impact on cell spreading compared to that in fibrous hydrogels. In nonfibrous hydrogels, cells are more likely to compress the matrix to expand the surrounding space for spreading or migration.[9,11d] Thus, lower matrix resistance as caused by stress relaxation or mechanical plasticity can facilitate cell spreading in nonfibrous matrix. On the contrary, in nanofibrous hydrogels such as collagen, cells can remodel the structure of the surrounding matrix by recruiting the fibers and thereby spread with the help of reaction generated by elastically deformed matrix fibers. Moreover, in nanofibrous hydrogels, a steric effect similar in nonfibrous hydrogels can be caused by material concentration, as cells spread more in collagen hydrogels with low concentration in our experiments (Figure 3d and Figure S5d,e, Supporting Information), highlighting the synergy between the two mechanisms in the regulation of cell morphology. Since most of the native ECM is inherently fibrous, our results, as a further evidence for cell-fibrous matrix interaction studies,[40] suggest that materials with fibrous structures should be preferred when mimicking the native ECM from mechanical aspects. Previously engineered tissue constructs primarily considered structure and matrix stiffness as the main biophysical cues.[41] Since mechanical plasticity can change in cancer tissues, fibrotic tissues and quite possibly in aged tissues, our findings highlight plasticity as an important parameter in tissue engineering, especially in engineering fibrotic disease models.

A recent work has demonstrated that cell-induced plastic remodeling of the ECM can open up microchannels in nanoporous matrices,[9] paving the way for cancer cells to migrate through confining microenvironments. Differently and interestingly, we found that high ECM plasticity is required for fibroblasts to keep in a low-tension state and maintain an inactive phenotype. While under a disease condition, the increased matrix crosslinking can lead to a decrease of matrix plasticity, which enables fibroblasts to establish a high-tension state, promoting fibroblast activation and fibrosis development. The effect of matrix plasticity on the development of fibrosis may precede the effect of stiffness in some scenarios. For instance, in myocardial infarction, the expression of LOX together with α-SMA starts to increase in the infarcted area 3 d after injury and peaked within 3–7 d.[6] Collagen, the widely recognized factor that enhances the stiffness of fibrotic tissue, starts to accumulate in the infarcted area at 7–21 d [42] and lead to the increase of matrix stiffness meanwhile.[43] Therefore, at the early stage of fibrosis (before excessive deposition of matrix proteins and the increase of matrix stiffness), the decrease in matrix plasticity as induced by increasing covalent crosslinking may be the main mechanical cue that promotes fibroblast activation. In addition, the latest findings suggest that CFs in the infarction area will lose their activation phenotype and be similar to the uninjured fibroblast phenotype 4 weeks after MI,[44] while at this stage matrix stiffness reaches a peak, suggesting that matrix stiffness may not be the determinate cue responsible for the activation of fibroblasts in vivo. This may guide researchers to re-examine the role of matrix stiffness in fibrosis, and inspire the development of novel therapeutic approach for treating fibrosis by exploiting the benefits of mechanobiology studies.

9. Experimental Section

Animal Experiments and Tissue Source: Wild-type Sprague–Dawley (SD) rats underwent proximal left coronary artery ligation for developing an MI model. Briefly, anaesthetized rats were connected to a rodent volume-controlled ventilator by intubation. The heart was exposed through a left thoracotomy followed by ligating the proximal left anterior descending coronary artery with 7-0 polypropylene suture. Myocardial ischemia was confirmed by regional cyanosis and ST-segment elevation. The incision was closed in layers with 4-0 silk continuous sutures. Rats were sacrificed after 4 weeks for mechanical test and staining. Approval was granted by the Institutional Review Board of The Second Affiliated Hospital of Xi'an Jiaotong University.

Collagen Hydrogels Preparation: Type I collagen was extracted from the tails of rats and dissolved in 0.1% acetic acid (Macklin) to a concentration of 6 mg mL^{-1}, following a protocol modified from literature.[45] Hydrogels were prepared on ice by neutralizing and diluting solution into a final concentration of 1, 3, or 5 mg mL^{-1} with 10X DMEM/Ham's F-12 medium

(DF-12; Gibco/Thermo Fisher Scientific), NaOH (Macklin) and di-distilled water (ddH_2O). Neutralized solution was immediately placed in an incubator (Thermo Fisher Scientific) to allow self-assembly at 37 °C for 40 min to form collagen hydrogels. For covalent crosslinking, self-assembled collagen hydrogels were immersed in DF-12 containing 0.1% microbial transglutaminase (mTG; Ajinomoto) for 1, 3, and 5 h at 37 °C and then washed three times with serum-free medium to remove residual mTG.

Mechanical Characterization: Rheology measurements were performed with an MCR 302 rheometer (Anton Paar), using 15 mm stainless steel parallel plate on temperature controlled peltier system at 25 °C. 200 mesh sandpapers (Norton Abrasives) were attached to the surface of rheometer to prevent the slippage of tissues or gels from the surface.

To test the rheology of collagen hydrogels, samples were prepared as discs with a diameter of 15 mm and a thickness of 2 mm. After self-assembly and covalent crosslinking, collagen hydrogels were soaked in phosphate buffered saline (PBS; MP Biomedicals) for 24 h to equilibrate before mechanical testing. At the beginning of test, the plate was slowly descended until reaching the normal force of ≈20 mN. The exposed edge of the collagen hydrogels between the two plates were sealed with mineral oil (Sigma-Aldrich) to minimize dehydration of the samples. Finally, a frequency sweep test was performed on the hydrogels at a strain of 1% and frequency from 0.1 to 10 rad s^{-1}. The storage modulus and loss modulus were calculated from the average of the modulus at a frequency of 0.25–2.5 rad s^{-1}, in which modulus kept an equilibrium value.

To characterize mechanical plasticity of the hydrogels, creep and recovery tests were applied. A constant stress of 20 Pa was applied to hydrogel samples for 500 s and then removed to recover strain for 5500 s. This timescale of recovery was enough to minimize transient effects caused by stress unloading. Plasticity degree was calculated as the value of final strain (γ_p) divided by the maximum strain (γ_{max}), i.e., γ_p/γ_{max}.

Creep and recovery tests were also carried out for tissue plasticity measurements. For native cardiac tissues, left ventricular wall of rats were trimmed into a nearly circular shape with a diameter of about 10 mm and a thickness of about 1.3 mm. A constant stress of 30 Pa was applied for 100 s and then relaxed for 1000 s. Changes in strain were recorded throughout the process.

Tensile experiments were carried out to verify the permanent deformation of collagen hydrogels under long-term recovery. Briefly, annular hydrogels were prepared in custom-made polymethyl methacrylate molds as shown in Figure S4a (Supporting Information). Using a tensile testing machine (Bose), tensile experiments were performed in PBS to minimize the influence of hydrogel weight (Figure S4b, Supporting Information). Hydrogels were first applied 30% strain at the rate of 0.1 mm s^{-1}, which was then held for 10 min. Next, hydrogels were removed from the machine and soaked in PBS for 10 min and 7 d. Residual strain was measured by vernier caliper and plasticity degree was calculated as the value of residual strain (ϵ_p) divided by the maximum strain (ϵ_{max}), i.e., $\epsilon_p/\epsilon_{max}$.

Swelling and Degradation: To characterize swelling ratio of the collagen hydrogels, wet weights of the hydrogels were measured immediately after preparation and after incubating in cell culture medium at 37 °C for 7 d. Swelling ratio was calculated as the ratio of the two measured weights. To characterize degradation of the hydrogels, the wet weights of hydrogels were measured once encapsulated with cells and after 7 d of cell culture to verify the degradation of hydrogels under cell culture condition.

Cell Culture: Primary cardiac fibroblasts (CFs) and lung fibroblasts (LFs) were isolated from neonatal SD rats as reported.[46] Primary cells were first seeded on plastic cell culture plates and passaged to second generation before encapsulation. For 3D culture, cell suspension was mixed with neutralized collagen solution to a density of 10^6 cells mL^{-1}. The solution was then deposited on a collagen-coated polydimethylsiloxane (PDMS) substrate to a thickness of 200 µm in order to ensure nutritional supply and prevent hydrogels from shrinking due to cell contractility. For 2D culture, collagen hydrogel was pre-prepared in six-well plates and soaked with serum-free medium overnight. Cells were plated at a low density of 5000 cells per well in order to minimize cell-cell contact.

CFs were cultured in DF-12 with 10% fetal bovine serum (Gibco/Thermo Fisher Scientific) and 1% pen/strep (Gibco/Thermo Fisher Scientific). LFs were cultured in Dulbecco's Modified Eagle Medium (DMEM; Gibco/Thermo Fisher Scientific) with 10% FBS and 1% pen/strep. All cells were cultured at 37 °C in 5% CO_2.

For inhibition treatments, all reagents or antibodies were added after the cells were encapsulated for 3 d and serum-starving for 12 h unless specifically stated in the text, using the following reagents: blebbistatin (50×10^{-3} M; Selleck, S7099), latrunculin A (0.3 µg mL^{-1}; Thermo Fisher Scientific, L12370), β1 integrin blocking antibody (5 µg mL^{-1}, Abcam, P5D2), losartan potassium (10×10^{-9} M; Selleck, S1359), rho activator II (1 µg mL^{-1}; Cytoskeleton, CN03-A), and GM6001 (10×10^{-6} M, Selleck, S7157).

For cell transfections, small interfering RNA (siRNA) transfections were done with Lipofectamine 2000 (Life Technologies) in Opti-MEM I reduced serum medium (Invitrogen) according to manufacturer's instructions. The target sequence of siRNA was 5′-GGUCAGAGAUACUUCUUAATT-3′ for rat YAP. siRNA transfections were performed on sparse fibroblast-containing hydrogels. siRNA transfections were repeated at least three times independently.

Immunohistochemistry and Immunofluorescence: For tissue staining, heart tissues from healthy and injured mice were fixed with formalin and preserved as paraffin-embedded samples. Immunohistochemistry and immunofluorescence stain were performed by standard protocols using the following antibodies: anti-α-SMA antibody (Boster, BM0002), anti-LOX-L2 antibody (Boster, BM5132), anti-TG2 antibody (Cell signaling technology, 3557S) and anti-Collagen I antibody (Boster, BA0325).

For cell staining, hydrogels were fixed in 4% paraformaldehyde (Bioshap) for 15 min and then washed three times with PBS. Cells were stained following standard immunofluorescence protocols directly after permeabilization with 0.5% Triton X-100 (Sigma-Aldrich) for 20 min. The following antibodies/reagents were used: α-SMA-FITC antibody (1:1000; Sigma-Aldrich, F3777), anti-paxillin antibody (1:200; Abcam, Y113) and anti-vinculin antibody (1:200; Abcam, EPR8185) collectively for focal adhesion staining, and YAP antibody (1:200; Abcam, 1674Y). Alexa Fluor 488 goat anti-rabbit secondary antibody (1:1000, Thermo Fisher Scientific, A11034) was used for counterstain. Rhodamine Phalloidin (1:1000, Thermo Fisher Scientific, R415) and DAPI (1 µg mL^{-1}, Sigma, D9542) were used to stain actin cytoskeleton and nucleus, respectively.

Microscopy and Image Analysis: An Olympus IX2-UCB was used to image nonfluorescent sections and an Olympus FV3000 confocal laser scanning microscope was used for fluorescence imaging. The fluorophores were excited by 405, 488, and 561 nm laser lines and the detection windows were set according to the labels' emission bands. A complete cross-sectional image of cardiac tissue was seamlessly spliced from a series of pictures. All grouped images were taken with keeping the capture parameters of target proteins (α-SMA, focal adhesion, YAP) consistently.

To measure cell spreading area, cell boundaries were thresholded manually based on the actin stain, and the spreading area was determined using ImageJ (NIH). For 3D cultured cells, spreading area was considered to be the projection of the cells along the z-axis. Images of DAPI/phalloidin/paxillin and vinculin antibody-stained cells were taken to quantify focal adhesions. Focal adhesions were identified manually and their number and length were quantified. To minimize the impact of artificial recognition, the background fluorescence intensity was subtracted as calculated from neighboring cell areas lacking adhesions by color gradation processing. The remaining stained regions on the cell boundaries were considered as focal adhesions. Images of DAPI/phalloidin/YAP antibody-stained cells were taken to quantify nuclear localization of YAP. Cell and nuclear boundaries were divided by threshold of each color channel. The YAP nuclear localization ratio was the sum of YAP signal intensity in the nuclear area divided by the sum of YAP signal intensity in the non-nuclear cytoskeleton area.

mRNA Expression Analysis: Fibroblast-containing hydrogels were removed from the PDMS substrates and RNA extraction kit (Tiangen) were used to harvest RNA from the hydrogels. A RevertAid First Strand cDNA Synthesis Kit (Thermo Fisher Scientific) was used to transcribe the extracted RNA into cDNA by polymerase chain reaction (PCR). Real-time PCR was conducted using SYBR Premix Ex Taq II (TaKaRa) and running on a Fast Real-Time PCR System (ABI, America). Relative gene expression was quantified using

the $2^{-\Delta\Delta Ct}$ method and internally normalized to glyceraldehyde-3-phosphate dehydrogenase (GAPDH). The sequences of primers were as follows: *GAPDH*: fwd 5′-CTTCTCTTGTGACAAAGTGGACAT-3′, rev 5′-CTTGCCGTGGGTAGAGTCAT-3′; *α-SMA*: fwd 5′-CGATAGAACACGGCATCATC-3′, rev 5′-CATCAGGCAGTTCGTAGCTC-3′.

Statistics: Statistical analyses were performed using the GraphPad Prism and charts was drawn by Origin Pro. Multiple comparisons among the four experimental groups with a single varying parameter were performed using one-way analysis of variance (ANOVA) with Bonferroni post hoc testing and the labels in charts only showed significant differences of the current group compared with the first group. Unless otherwise specified, *, **, ***, and **** indicate significant difference with $p < 0.05$, $p < 0.01$, $p < 0.001$ and $p < 0.0001$ by one-way ANOVA, respectively. #### indicates significant difference with $p < 0.0001$ by Spearman's rank correlation. ns, indicates not significant. All data are shown as mean ± SD. For box chart, the box plots show 25/50/75th percentiles and whiskers show 5/95th percentiles and the black dots represent the mean of the data. All the sample size was showed in figure legend. No statistical methods were used to predetermine sample size.

Supporting Information

Supporting Information is available from the Wiley Online Library or from the author.

Acknowledgements

This work was financially supported by the National Natural Science Foundation of China (11872298, 11532009, 11621062, and 31900939), the China Postdoctoral Science Foundation (2019T120895), and the Fundamental Research Funds for the Central Universities (Z201811336).

Conflict of Interest

The authors declare no conflict of interest.

Author Contributions

Y.J., G.H., and F.X. designed the experiments. Y.J., L.N., and H.Z. conducted cell and molecular experiments. Y.W., J.Q., and J.T. developed the model and ran simulations. L.N., X.Z., and D.G. carried out animal experiments. Y.J., G.H., F.X., and T.J.L. analyzed the data. H.Z. and X.Z. helped with figure edition. Y.J., Y.W., J.Q., F.X., and G.H. wrote the manuscript. All authors edited the manuscript.

Data Availability Statement

The data that support the findings of this study are available from the corresponding author upon reasonable request.

Keywords

cell traction, fiber networks, fibrosis, mechanical plasticity, nanofibrous matrix

Received: October 22, 2020
Revised: January 16, 2021
Published online: January 29, 2021

[1] a) S. Munster, L. M. Jawerth, B. A. Leslie, J. I. Weitz, B. Fabry, D. A. Weitz, *Proc. Natl. Acad. Sci .USA* **2013**, *110*, 12197;. b) C. Storm, J. J. Pastore, F. C. MacKintosh, T. C. Lubensky, P. A. Janmey, *Nature* **2005**, *435*, 191.
[2] H. Mohammadi, E. Sahai, *Nat. Cell Biol.* **2018**, *20*, 766.
[3] a) R. Don C, B. P. Darwin, H. Joseph A, *N. Engl. J. Med.* **2015**, *372*, 1138; b) T. A. Wynn, *J. Exp. Med.* **2011**, *208*, 1339.
[4] a) J.-S. Silvestre, C. Heymes, A. Oubénaïssa, V. Robert, B. Aupetit-Faisant, A. Carayon, B. Swynghedauw, C. Delcayre, *Circulation* **1999**, *99*, 2694;. b) M. Selman, T. E. King, A. Pardo, *Ann. Intern. Med.* **2001**, *134*, 136;. c) S. L. Friedman, *Nat. Rev. Gastroenterol. Hepatol.* **2004**, *1*, 98.
[5] a) F. Klingberg, M. L. Chow, A. Koehler, S. Boo, L. Buscemi, T. M. Quinn, M. Costell, B. A. Alman, E. Genot, B. Hinz, *J. Cell Biol.* **2014**, *207*, 283;. b) D. C. Rockey, C. N. Housset, S. L. Friedman, *J. Clin. Invest.* **1993**, *92*, 1795.
[6] J. González-Santamaría, M. Villalba, O. Busnadiego, M. M. López-Olañeta, P. Sandoval, J. Snabel, M. López-Cabrera, J. T. Erler, R. Hanemaaijer, E. Lara-Pezzi, *Cardiovasc. Res.* **2015**, *109*, 67.
[7] N. Shweke, N. Boulos, C. Jouanneau, S. Vandermeersch, G. Melino, J. C. Dussaule, C. Chatziantoniou, P. Ronco, J. J. Boffa, *Am. J. Pathol.* **2008**, *173*, 631.
[8] a) D. C. Sane, J. L. Kontos, C. S. Greenberg, *Front. Biosci.* **2007**, *12*, 2530;. b) H. V. Barry, R. D. Spangler, S. Mccauley, H. M. Rodriguez, M. Oyasu, A. Mikels, M. Vaysberg, H. Ghermazien, C. Wai, C. A. Garcia, *Nat. Med.* **2010**, *16*, 1009.
[9] K. M. Wisdom, K. Adebowale, J. Chang, J. Y. Lee, S. Nam, R. Desai, N. S. Rossen, M. Rafat, R. B. West, L. Hodgson, O. Chaudhuri, *Nat. Commun.* **2018**, *9*, 4144.
[10] S. Nam, J. Lee, D. G. Brownfield, O. Chaudhuri, *Biophys. J.* **2016**, *111*, 2296.
[11] a) E. E. Charrier, K. Pogoda, R. G. Wells, P. A. Janmey, *Nat. Commun.* **2018**, *9*, 449;. b) O. Chaudhuri, L. Gu, M. Darnell, D. Klumpers, S. A. Bencherif, J. C. Weaver, N. Huebsch, D. J. Mooney, *Nat. Commun.* **2015**, *6*, 6364;. c) O. Chaudhuri, L. Gu, D. Klumpers, M. Darnell, S. A. Bencherif, J. C. Weaver, N. Huebsch, H. Lee, E. Lippens, G. N. Duda, *Nat. Mater.* **2016**, *15*, 326;. d) H. P. Lee, L. Gu, D. J. Mooney, M. E. Levenston, O. Chaudhuri, *Nat. Mater.* **2017**, *16*, 1243.
[12] T. S. Lai, Y. Liu, T. Tucker, K. R. Daniel, D. C. Sane, E. Toone, J. R. Burke, W. J. Strittmatter, C. S. Greenberg, *Chem. Biol.* **2008**, *15*, 969.
[13] T. A. Wynn, *J. Pathol.* **2010**, *214*, 199.
[14] a) I. Stachel, U. Schwarzenbolz, T. Henle, M. Meyer, *Biomacromolecules* **2010**, *11*, 698;. b) D. Y. S. Chau, R. J. Collighan, E. A. M. Verderio, V. L. Addy, G. Martin, *Biomaterials* **2005**, *26*, 6518.
[15] P. S. Van, Y. Shafieyan, B. Hinz, *J. Mol. Cell. Cardiol.* **2016**, *93*, 133.
[16] a) A. R. Cameron, J. E. Frith, J. J. Cooper-White, *Biomaterials* **2011**, *32*, 5979;. b) S. V. Plotnikov, A. M. Pasapera, B. Sabass, C. M. Waterman, *Cell* **2012**, *151*, 1513;. c) C. E. Chan, D. J. Odde, *Science* **2008**, *322*, 1687.
[17] a) K. Nicholas Agung, E. S?Ren, R. Raj, *J. Chem. Phys.* **2012**, *136*, 02B604; b) E. Ban, J. M. Franklin, S. Nam, L. R. Smith, H. Wang, R. G. Wells, O. Chaudhuri, J. T. Liphardt, V. B. Shenoy, *Biophys. J.* **2018**, *114*, 450.
[18] J. Kim, J. Feng, C. A. R. Jones, X. Mao, L. M. Sander, H. Levine, B. Sun, *Nat. Commun.* **2017**, *8*, 842.
[19] a) R. G. Wells, *J. Clin. Gastroenterol.* **2010**, *13*, A24; b) E. Hadjipanayi, V. Mudera, R. A. Brown, *J. Tissue Eng. Regener. Med.* **2010**, *3*, 77.
[20] a) C. M. Madl, B. L. Lesavage, R. E. Dewi, C. B. Dinh, R. S. Stowers, M. Khariton, K. J. Lampe, D. Nguyen, O. Chaudhuri, A. Enejder, *Nat. Mater.* **2017**, 16;. b) K. Sudhir, G. Murat, W. R. Legant, D. M. Cohen, C. S. Chen, J. A. Burdick, *Nat. Mater.* **2013**, *12*, 458.

[21] C. T. Mierke, D. P. Kollmannsberger PZitterbart, G. Diez, T. M. Koch, S. Marg, W. H. Ziegler, W. H. Goldmann, B. Fabry, *J. Biol. Chem.* **2010**, *285*, 13121.
[22] a) P. Kollmannsberger, C. M. Bidan, J. W. C. Dunlop, P. Fratzl, V. Vogel, *Sci. Adv.* **2018**, *4*, eaao4881;. b) H. Xiangwei, Y. Naiheng, V. F. Fiore, T. H. Barker, S. Yi, S. W. Morris, D. Qiang, V. J. Thannickal, Z. Yong, *Am. J. Respir. Cell Mol. Biol.* **2012**, *47*, 340;. c) R. G. Wells, D. E. Discher, *Sci. Signaling* **2008**, *1*, pe13.
[23] R. Oria, T. Wiegand, J. Escribano, A. Elosegui-Artola, J. J. Uriarte, C. Moreno-Pulido, I. Platzman, P. Delcanale, L. Albertazzi, D. Navajas, *Nature* **2017**, *552*, 219.
[24] G.-K. Xu, C. Yang, J. Du, X.-Q. Feng, *J. Biomech.* **2014**, *47*, 1479.
[25] a) Z. Yunzeng, A. Hiroshi, Q. Yingjie, S. Masanori, T. Hiroyuki, M. Tohru, M. Noriko, I. Koji, Z. Weidong, K. Sumiyo, *Nat. Cell Biol.* **2004**, *6*, 499;. b) K. W. Yong, Y. Li, F. Liu, B. Gao, T. J. Lu, W. A. B. Wan Abas, W. K. Z. Wan Safwani, B. Pingguan-Murphy, Y. Ma, F. Xu, G. Huang, *Sci. Rep.* **2016**, *6*, 33067.
[26] P. Chen, V. B. Shenoy, *Soft Matter* **2011**, *7*, 355.
[27] J. Tianrong, L. Li, R. C. M. Siow, L. Kuo-Kang, *J. R. Soc., Interface* **2015**, *12*, 20141365.
[28] a) H. Georg, D. Sirio, P. Stefano, *Nat. Rev. Mol. Cell Biol.* **2012**, *13*, 591; b) T. Panciera, L. Azzolin, M. Cordenonsi, S. Piccolo, *Nat. Rev. Mol. Cell Biol.* **2017**, *18*, 758.
[29] B. Piersma, S. de Rond, P. M. N. Werker, S. Boo, B. Hinz, M. M. van Beuge, R. A. Bank, *Am. J. Pathol.* **2015**, *185*, 3326.
[30] J. Y. Shiu, L. Aires, Z. Lin, V. Vogel, *Nat. Cell Biol.* **2018**, *20*, 262.
[31] S. Dupont, L. Morsut, M. Aragona, E. Enzo, S. Giulitti, M. Cordenonsi, F. Zanconato, J. L.e Digabel, M. Forcato, S. Bicciato, *Nature* **2011**, *474*, 179;.
[32] O. Chaudhuri, J. Cooper-White, P. A. Janmey, D. J. Mooney, V. B. Shenoy, *Nature* **2020**, *584*, 535.
[33] S. R. Caliari, S. L. Vega, M. Kwon, E. M. Soulas, J. A. Burdick, *Biomaterials* **2016**, *103*, 314.
[34] J. Y. Lee, J. K. Chang, A. A. Dominguez, H.-p. Lee, S. Nam, J. Chang, S. Varma, L. S. Qi, R. B. West, O. Chaudhuri, *Nat. Commun.* **2019**, *10*, 1.
[35] W. A. Border, N. A. Noble, *N. Engl. J. Med.* **1994**, *331*, 1286.
[36] K. W. Yong, Y. Li, F. Liu, B. Gao, T. J. Lu, A. W. Wan, S. W. Wan, B. Pingguan-Murphy, Y. Ma, F. Xu, *Sci. Rep.* **2016**, *6*, 33067.
[37] J. M. Grolman, P. Weinand, D. J. Mooney, *Proc. Natl. Acad. Sci. USA* **2020**, *117*, 25999.
[38] D. D. Mckinnon, D. W. Domaille, J. N. Cha, K. S. Anseth, *Adv. Mater.* **2014**, *26*, 865.
[39] J. Lou, R. Stowers, S. Nam, Y. Xia, O. Chaudhuri, *Biomaterials* **2017**, *154*, 213.
[40] a) L. A. Smith, P. X. Ma, *Colloids Surf., B* **2011**, *21*, 10243; b) M. S. Hall, F. Alisafaei, E. Ban, X. Feng, C.-Y. Hui, V. B. Shenoy, M. Wu, *Proc. Natl. Acad. Sci. USA* **2016**, *113*, 14043; c) X. Cao, E. Ban, B. M. Baker, Y. Lin, J. A. Burdick, C. S. Chen, V. B. Shenoy, *Proc. Natl. Acad. Sci. USA* **2017**, *114*, E4549.
[41] G. Huang, F. Li, X. Zhao, Y. Ma, Y. Li, M. Lin, G. Jin, T. J. Lu, G. M. Genin, F. Xu, *Chem. Rev.* **2017**, *117*, 12764.
[42] a) J. W. Holmes, T. K. Borg, J. W. Covell, *Annu. Rev. Biomed. Eng.* **2005**, *7*, 223;. b) M. Dobaczewski, C. Gonzalez-Quesada, N. G. Frangogiannis, *J. Mol. Cell. Cardiol.* **2010**, *48*, 504.
[43] Z. Shuning, S. Aijun, M. Hong, Y. Kang, Z. Ning, S. Li, Z. Chunyu, Z. Yunzeng, G. Junbo, *J. Cell. Mol. Med.* **2011**, *15*, 2245.
[44] A. L.e Bras, *Nat. Rev. Cardiol.* **2018**, *15*, 379.
[45] R. Navneeta, H. Jason, C. Marie-France, C. J. Doillon, M. Diego, *Nat. Protoc.* **2006**, *1*, 2753.
[46] a) S. H. Phan, J. Varani, D. Smith, *J. Clin. Invest.* **1985**, *76*, 241;. b) B. W. Doble, Y. Chen, D. G. Bosc, D. W. Litchfield, E. Kardami, *Circ. Res.* **1996**, *79*, 647.